Negative differential resistance in photoassisted field emission from Si nanowires

M. Choueib, A. Derouet, P. Vincent, A. Ayari, S. Perisanu, P. Poncharal, Costel Sorin Cojocaru, R. Martel, S. Purcell

Negative Differential Resistance in Photo-Assisted Field Emission from Si Nanowires

M. Choueib,[1,2] A. Derouet,[2] P. Vincent,[2] A. Ayari,[2] S. Perisanu,[2] P. Poncharal,[2] C. S. Cojocaru,[3] R. Martel,[1] and S. T. Purcell[2]

[1)] *Département de chimie, Université de Montréal, Montréal, Québec H3T 1J4, Canada*

[2)] *Institut Lumière Matière, Université Lyon 1, CNRS, UMR 5306, F-69622 Villeurbanne, Cedex, France*

[3)] *Ecole Polytechnique LPICM, UMR 7647, F-91128 Palaiseau, France*

(*Electronic mail: stephen.purcell@univ-lyon1.fr)

(*Electronic mail: r.martel@umontreal.ca)

(Dated: 7 January 2022)

Field-emission (FE) from semiconducting nanowires (NWs) is studied for expanding electron gun performances and functionality in terms of stability, brightness and pulsed emission. Here we report on a pronounced and robust double negative differential resistance (NDR) in the FE IV characteristics measured during photo-assisted field emission experiments on highly crystalline p-type silicon nanowires (NWs). The main feature is a double NDR in the current saturation regime, which can be modulated by both temperature and light intensity. These results contrast with previous FE studies in which only barely noticeable single NDR was reported. Several mechanisms for the physical explanation of the NDR are currently under consideration : photo-generated carrier instabilities in the depletion region, which give rise to a pulsed space-charge current in the nanowire or tunneling through a double quantum well formed by confinement at the NW apex. Because NDRs are signatures of pulsed currents, these results suggest new functionalities for which pulsed electron sources can potentially be achieved at high repetition rates.

INTRODUCTION

There is a growing interest in developing time modulated and ultrashort pulsed electron sources for fundamental studies on dynamical processes in *e.g.* electron microscopes[1,2] and on field-emission processes induced by ultrafast lasers[3,4]. Scientific and technical advances on pulsed sources can also find use in applications such as diffractometers[5–7], radio frequency amplifiers and X-ray imaging systems[8,9]. In most experiments, the electron emitter is a photo-cathode activated by ultra-short laser pulses operating at kHz to MHz repetition rates, which photo-emits electron packets of a very short time duration (sub-ps). This scheme requires an important infrastructure, *e.g.* a short wavelength and pulsed laser source, and it is therefore not well adapted to many instruments requiring compact sources. Electron emitters based on field-emission provide an alternative for making well-defined point sources having high brightness, low energy distribution, and stable emission. However, there is currently no known field-emitting source providing ultra-fast oscillating electron emission that can be powered cheaply by a *dc* energy source, that is to say a self-oscillating field emitter[10].

In this work, we test new ideas targeting the promotion of oscillatory (pulsed) emission during field-emission (FE) of low-doped semiconducting nanowires (NWs) under continuous laser excitation. This research builds upon the well-developed field of high-speed oscillating devices[11] with notorious examples such as the transferred-electron devices in the momentum space, also called the Gunn diode[12], or in the real-space using heterostructures[13], with examples such as the resonant tunneling double barrier diodes (DBDs)[14] and the quantum-well (QW) p-i-n photo-diodes[15]. A low-doped semiconducting channel is usually inserted in the core of these device structure to enable charge fluctuations induced by the electric field, and this gives rise during operation to domains of excess (negative) and depleted (positive) electrons within the channel[16]. The presence of a negative differential resistance (NDR) in the current-voltage curves (IVs) is a hallmark of such charge instabilities, which form transient states known to induce self-oscillations. In the context of field-emission, NDRs have been previously explored experimentally[17–21] and theoretically[22–24] using various structures based on QW heterostructures and surface states, but the signatures of the NDR are generally weak, of unproven reproducibility, are from nanostructured surfaces with the real emitters not identified, are characterised only with basic IV measurements, and lack the control needed to promote a self-oscillation.

Here, we report on a double N-shape NDR in the photo-assisted field-emission *IV* characteristics of individual highly crystalline Si nanowires (NWs). The NDR features are measured under continuous laser intensity at λ=514nm and shown to depend on both light intensity (Φ) and temperature. Experiments on different NWs and measurements of I(V,T,Φ) curves and total energy distributions (TED) during FE in ultrahigh vacuum (UHV), support a mechanism based on a charge fluctuations forming transient states within the depletion zone of the NW.

I. EXPERIMENTAL DETAILS

A. Si Nanowires and their pre-preparation

Si NWs were grown at 540°C by chemical vapor deposition (CVD) in a homemade chamber according to a vapor-liquid-solid (VLS) process. The CVD growth was carried out from

a catalyst layer made of a layer of Au (10nm) deposited onto a TiN(30 nm)/Si wafer and using silane (SiH_4) as a precursor gas diluted in 10% hydrogen at a total pressure of 15 mbar under a total flow of 100 sccm. CVD growth was assisted by a hot-filament maintained at 1900°C and was carried out in a flow of H_2 gas, as detailed elsewhere[25].

Photo-assisted FE measurements were carried out on two individual silicon nanowires (NW1: diameter d = 92nm, length $L = 11.5\mu$m and NW2: d = 100 nm, $L = 20\mu$m). Their mechanical resonance frequencies were measured in situ by FE[26] to be f = 119kHz and 107 kHz respectively. The NWs were attached by conductive carbon glue to tungsten tips (Figure 1-c). The VLS process lead to an unintentional p-doping ($N_a = \sim 2 \times 10^{15}/cm^{-3}$)[27]. Transmission Electron Microscope (TEM) images of the NWs (See Figures S1 and S2, Supplementary Material) show that they had a highly crystalline core covered with a 10 nm oxide passivation layer all along the sidewall. The apex of NW1 (Figure 1b) was rounded using *in-situ* field-induced atomic evaporation in a TEM at +1200V bias applied to a gold ball placed in proximity, which induces a local field for atomic Si evaporation of about 40 V.nm^{-1}.[28] Such a process produces a close to atomically clean Si surface on the apex. However its consequent exposure to ambient atmosphere for the transfer to the FE system (see next) undoubtedly creates a 1 nm scale native oxide. The apex of NW2 was used "as is" and consists of a rounded silicon tip containing the gold nanoparticle catalyst (See Figures S1 and S2, Supplementary Material). The dependence of FE from NW2 on voltage and temperature was previously presented in reference[27].

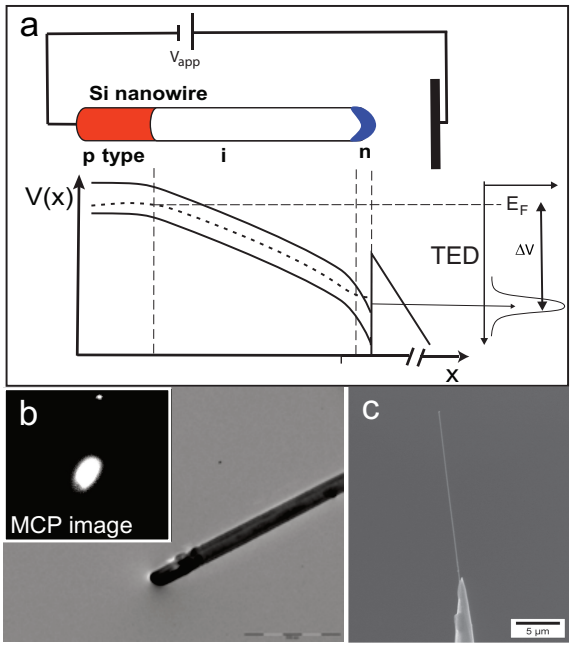

FIG. 1. *a*, Scheme of the voltage drop and Fermi level (dotted line) in the silicon nanowire induced by the electric field ξ in the saturation region: the doping is n-type (or degenerate) at the tip followed with a depletion region (i : intrinsic) and the p-type body. *b*, Transmission Electron Microscopy (TEM) image of NW1 zoomed on the rounded tip obtained after field-induced atom desorption for 5 min. The scale is 500 nm. Inset: A typical FE image of a Si NW with rounded apex acquired by the microchannel plate detector *c*. Scanning electron microscopy of Si NW2 (diameter d=100nm and length L=20μm) attached to a tungsten tip.

B. Field emission setup and in-situ NW treatments

All FE measurements were carried out at a base pressure of 2×10^{-10} Torr in a dedicated ultrahigh vacuum system for which a schema is given in the supplementary information (Fig. S6). The NWs were mounted on W tips welded to a resistive W wire loop, which allows the NW temperature to be varied by Joule heating from 100 to 2000K, quantified with a micro-pyrometer and thermocouples. The distance of the tip to the quadropole extraction anode is about 2 mm. The setup is equipped with a micro-channel plate (MCP) detector, an electron counter sensitive down to 10^{-20}A and an electron energy analyzer (VG Scientific CLAM-2), which provides the total energy distribution (TED) from which the Fermi level at the NW apex can be determined with respect to that of the support tip, and thus the voltage drop ΔV along the NW (Figure 1-a). Combined with the measured total current, these measurements are the equivalent of a two point transport measurement, which has allowed us to identify the carrier transport mechanisms in these individual semiconducting NWs. Continuous wave (CW) optical excitation was performed using illumination from one side of the NWs by an Ar^+ laser (λ=514 nm) focused with a standard optical setup mounted outside the vacuum chamber in front of a viewport. Appropriate attenuators, focal spot size measurements and intensity calibrations were used.

We have previously reported on the FE properties of Si NWs from the same batches and extensively discussed the nonlinear FN Plots of the IVs obtained after passivation, which show a characteristic large saturation zone in current, similar to reverse bias diodes, due to a space charge region (SCR) that opens out from the NW apexes in the sub nA range[27]. Furthermore the saturation level rises exponentially with temperature (see below) and there was no significant difference between the Au or Si terminated nanowires. Although no dopants were included in the synthesis, the IVs obtained with the NWs are consistent with what is expected for modest concentration p-doped NWs as measured[29] and predicted for the FE theory of p-doped semiconductors[30]. The saturation plateaus of NW2 were substantially degraded by a too strong laser intensity (2kW/cm^2) before the photo-assisted measurements but this actually allows us to demonstrate the existence of our phenomena for very different NW conditions.

Prior to FE measurements, the NWs were first annealed a few times in UHV at 500 °C during 5 min to remove mobile contaminants and then exposed at 400 °C for 5 min to an atomic hydrogen beam produced by a nearby hot (white emission) W filament and 10^{-5} torr of H_2[27]. These steps clean and passivate the oxide layer of the NWs, ensuring stable emission and better saturation characteristics in the IV curves. Hydrogen passivation can recover to a certain degree the saturation

lost by excess heating[27]. The rounded apex provided for both NWs a reasonable directionality to the electron beam. The integrity of each NW was fully probed before, during and after the experiments, using Fowler-Nordheim plots to ensure consistency of field amplification and mechanical resonance frequencies. These showed that the NW lengths were always conserved.

II. RESULTS

A. Measurement of Negative Differential Resistance

The room temperature *IV* plots for NW1 and NW2 under a continuous laser intensity at λ=514nm are shown in Figure 2-a and 2-b, respectively, and in Figure S3 (Supplementary Material) on a log scale. Of central interest for this study are the *IV* plots in the saturation region with increasing laser power density, Φ. First note that for both NWs, the *IV* curves in the saturation region show a high sensitivity to laser light: increasing the light intensity shifts up the saturated current without changing the slope, and increases also the onset of saturation toward higher voltages. The main result of this article is that the photo-assisted *IVs* of both NWs exhibit two sharp peaks at high light intensity, the so-called N-shaped NDRs. They are very stable and present almost no hysteresis between forward and backward bias scans (Figure S4, Supplementary Material). The rest of this article aims to better characterize this phenomena and discuss two frameworks for its eventual explanation.

There is a significant different sensitivity to laser intensity for NW1 and NW2 (after the laser modification mentioned above). While the emission currents at an applied voltage of 350 V are comparable in the dark, the current change at 200 mW/cm^2 is 14x for NW1 and only 1.2x for NW2. In other words, it takes about 14x more light intensity for NW2 to reach the same current as NW1 in the *IV* curves and the situation worsens at higher bias. This difference comes from the surface passivations of the two NWs (see next). What is remarkable is that the NDRs are present in both quite different NWs. The phenomena appears to be robust.

Another important aspect is that with increasing laser intensity these NDR peaks shift linearly in voltage and increase strongly in amplitude. For example, increasing the intensity on NW1 from 49 to 195 mW/cm^2 induces a 18V shift to the first NDR and an increase in amplitude of 3 pA to 18 pA. The second NDR follows generally a similar trend as both NDRs are located in the saturation region where the emission is limited by generation-recombination current (I_{GR}). Because of the steeper *IV* slope for NW2 in the dark and the poor response to laser light, the NDRs are more difficult to visualize, but the behavior is roughly the same (Figure S5, Supplementary Material). We have previously shown that steeper slopes in the saturation region of the *IV* is due to current leakages associated to the presence of traps at the Si/SiO$_2$ interface[27].

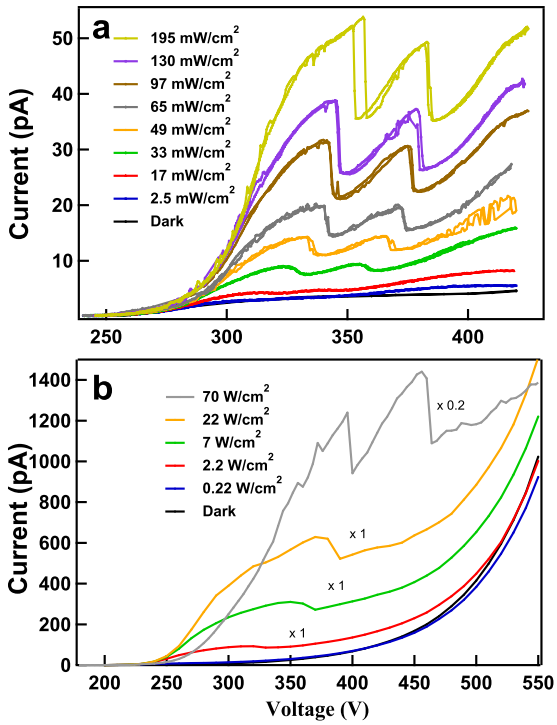

FIG. 2. Current-Voltage plots with increasing laser intensity for NW1 (a) and NW2 (b). In the saturation regions, the current is highly sensitive to laser intensity as predicted by theory for field emission from semiconductors and features two negative differential resistance peaks.

B. Temperature effects and internal voltage drop

Next we explore more thoroughly the properties of the N-shaped NDRs, hereafter labeled NDR1 and NDR2, of NW1 using I(V,T,Φ) experiments and TED measurements. Figure 3-a presents the *IV* curves of NW1 in the dark at different temperatures to more fully reveal the saturation region without laser excitation. The saturation current is clearly thermally activated with a fitted activation energy of E$_a$=0.54 eV, i.e. roughly half of the bandgap of silicon. This value is typical for such Si NW and ascribed to Au impurities (atoms) deposited during VLS growth, which induce mid-gap states. As discussed in our previous work, these states are driving the dynamics of the generation-recombination (GR) processes in the SCR of these Si NWs[27].

An early signature of the first NDR appears in the saturated *IV* of Figure 3-a as a small amplitude kink shifting to higher voltage with temperature (see arrows). The shift of the NDRs with *T* is more clearly seen in Figure 3b under 65 mW/cm^2 excitation. Increasing *T* reduces also the amplitude of both NDRs from a maximum of $\sim$5 pA at room temperature to near zero at T$>$ 500K. Increasing temperature linearly shifts the NDRs to higher applied voltages (V_{app}) with a slope of $\sim$0.2V/K.

When varying the conditions it became apparent that the shift in voltage and the reduction in amplitude with *T* can

be compensated with light intensity. As shown in Figure 3-c, the conditions that match similar amplitudes and positions for both NDRs at room temperature is found at 100K when increasing the laser intensity from 49 to 653 mW/cm^2. Surprisingly, these curves present almost the same NDR peaks (amplitude and position) but under very different laser powers. As discussed below, these experiments demonstrate that a gradient of temperatures in the NW is not required to generate the NDRs. Furthermore, the shifting in voltage of the NDRs with increasing laser fluence and temperature suggests a mechanism that involves photo-generated carriers. That is, sharper transitions develop for the NDRs at the lower temperature and higher light intensity, and hence it is fair to deduce at this point that the mechanism is most likely related to the minority carriers promoted by light excitation.

Further insight into the NDR mechanism was gained by measuring TEDs of the emitted electrons from NW1 under different conditions with a hemispherical electron energy analyzer located in the same UHV system (see §Field emission setup and in-situ NW treatments). As can be seen in Figure 4, the TEDs shift with the applied voltage (and increasing emission current) to lower energy, which is consistent with an increasing penetration of the electric field into the NW. It was previously shown that this voltage drop is due to an increase of the width, W, of the depletion region (or SCR) in the NW channel, generating an internal field of about 2.5 V/μm[27,31]. An important observation here is the presence of a second peak at applied voltages near that of the NDR regions, as highlighted in red. The occurrence of the twin peaks indicate that two distinct emitting states are being formed at voltages in the NDR regions. (Note that the peaks continue to shift linearly through the NDR. The red curves are separated by smaller voltage steps). Thus associated with the NDR loss of current is a simultaneous sudden increase in the voltage drop inside the NW. In fact two solutions for the nanowire ΔV can exist at one total applied voltage. Furthermore the NW actually flip flops back and forth randomly in time on the msec timescale between the two peak positions during the transition part of the voltage scan where the two peaks exist. A consequence of this oscillating behaviour is the extra features (noise) within each peak, which are due to short episodes of missing signals during the spectra scan when the NW switches to the other state. This is reminiscent of the first comments of Gunn when he discovered the Gunn effect. The instabilities are also highlighted by a strong noise in the spectra near the NDR regions as well as a significant broadening of the peak (see insets of Fig. 4 and a measure of the noise of the signal in Fig. S6, Supplementary Material). We do not yet have access to the switching event (or time) itself but one may be tempted to relate it to the broadening.

The instabilities in the emitted current under 97mW/cm^2 light intensity are further detailed by plotting the current as a function of both the applied voltage and the voltage drop ΔV measured by the electron analyzer (Fig. 5-a). The band situation giving this ΔV is illustrated in Figure 1a. Near the first NDR, the current reaches a maximum and starts to oscillate between two emission peaks, one of higher (before NDR) and another of lower emission currents (after the NDR). The current stabilizes to a minimum noise value past a threshold voltage, which is an important signature of these NDRs. Past the NDR1, the current increases again with applied voltage and keeps an apparent stability until the next region of instability (NDR2). The voltage drop associated with these transitions is illustrated in Figure 5-b as a function of the applied voltage. The ΔV grows linearly with applied voltage and increases suddenly in the NDR regions by about 3 V for NDR1 and 2 V for NDR2. As detailed in Figure 5c, the transitions are associated with a broadening of the TED peaks. The full width at half maximum (FWHM) grows with voltage from about 0.5 eV up to about 1 eV at the instability. There is a suddenly drop of the

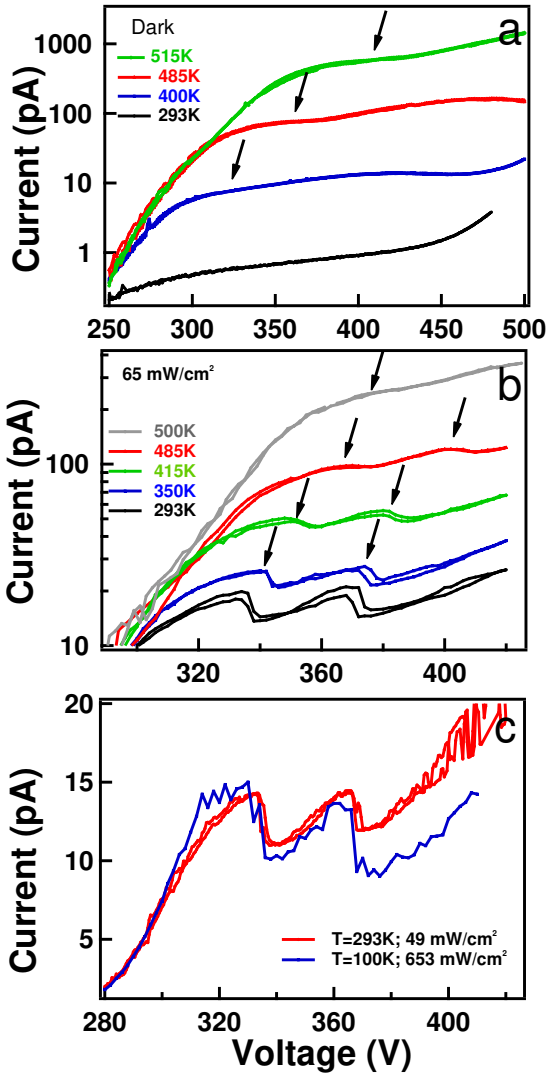

FIG. 3. Temperature dependence of the IV curves for NW1. (a) Current-Voltage plots with increasing temperature. (b) Effect of temperature under a 65 mW/cm^2 laser intensity. Arrows in (a) and (b) point to apparent NDR features and highlight a shift of the NDRs to higher voltage with T up until T = 500K. (c) Two NDR curves taken at 100K and 293K under laser fluence of 49mW/cm^2 (red) and 653mW/cm^2 laser (blue), respectively, to match the same level of current for both.

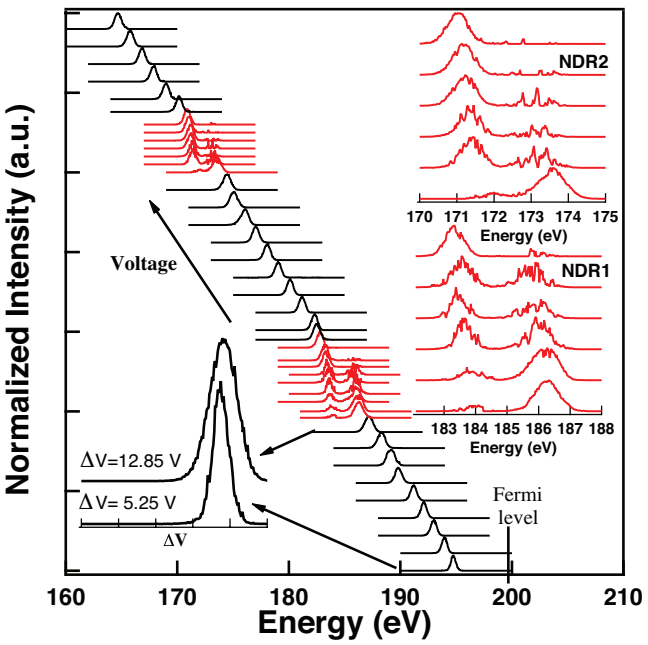

FIG. 4. Series of TEDs for the NW1 at a power density of 65mW/cm^2 showing a peak shift to lower energy with increasing applied voltage. One notices the appearance of a second peak (red zone) when we reach the NDR regions. Insets: zoom on NDR1 and NDR2 regions (red) showing clearly two peaks and an oscillation between the peaks in the vicinity of the NDR.

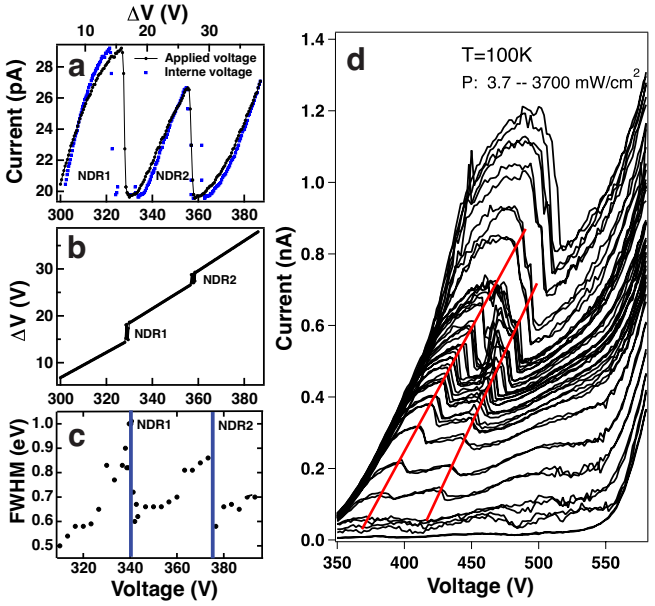

FIG. 5. Further details of the current instabilities and the negative differential resistance of NW1 under 97mW/cm^2 light intensity at room temperature. (a) Current as a function of voltage drop and applied voltage. (b) Voltage drop (internal voltage) as a function of the applied voltage highlighting the sudden voltage drop at NDRs. (c) Half width at half maximum (FWHM) of the emission peak vs. applied voltage. (d) Evolution of the NDR at 100K and higher laser fluence.

FWHM past the instability back to a value of about 0.6 eV.

Finally it is instructive to present a full series of IVs measured at 100K for which we can use stronger laser powers. As shown in Fig. 5(d) the two NDRs are present at lower intensity and get closer and eventually merge into one even more pronounced NDR with the higher intensity. Note that the NDR now reaches the nA range and this is not a limit.

III. DISCUSSION

Considering the high sensitivity of the FE current to temperature, we have thoroughly tested if these NDRs are due to thermal effects. Indeed, the total current is mostly related to the carrier concentration, n_i, which in turn depends on temperature T, as $n_i(T) \propto exp\frac{-E_{gap}}{2k_BT}$, where E_{gap} is the bandgap and k_B is the Boltzmann constant. A temperature gradient is therefore a possible driving source of the non-linearity in the response reported above. However, the shape and amplitude of the NDRs in Figure 3-b are negatively affected by temperature, which suggests that it is not thermal. Note that the laser intensity was kept rather low and the temperature profile is rather uniform and mostly set by thermal conduction from the W tip in contact with the NW. We tested other conditions that could induce a significant temperature gradient across the NW, but we reached the same conclusion. It was, for instance, possible to generate a non-uniform temperature gradient across the NW using laser heating on one side of the NW and thermal contact on the other side with the W tip acting as a heat sink[32]. Figure 3-c presents a direct comparison of two NDR shapes obtained when the W tip is placed at 100K and room temperature. By boosting significantly the laser intensity on the NW at 100K, we could compensate the thermal loss of current, but this generated no obvious change in the IV compared to room temperature. These results show no or little effect of temperature gradients on the NDR shapes. This is consistent with a rough estimate of the temperature gradients in those conditions, which are found to be negligible (Section 3, Supplementary Material). From those experiments, we can safely conclude that the mechanism behind the NDRs is not thermal.

Several nonthermal mechanisms may explain the double NDR features observed here. The two main models we are presently considering are depicted in Figure 6 : i) Photogenerated carriers in the depletion region induce space-charge current build-ups in the nanowire (Fig. 6-a) and ii) A double quantum well[22,33,34] is formed by confinement near the Si nanowire apex (Fig. 6-b). The latter would essentially depend on the distribution of the surface states of the Si NW, or within the residue of the native oxide, under strong electric fields, while the former implies that instabilities lead to a transient state causing an accumulation of excess positive charges in the depletion region. This space-charge would cause a transient (unstable) electric field within the depletion region of the NW and result in oscillating currents.

The resonant tunnelling in a double QW is a mechanism

based on a mixed, then sequential, resonant tunnelling across multiple barriers; the voltage at the apex could shift the resonant states in and out resonance, giving the NDR (see Fig. 6 b). This mechanism is consistent with the double feature, NDR1 and NDR2, seen in the *IV* and it is inspired by the realization that surface states at the tip are generally important to explain the FE properties of most emitters. Simulations for the IVs of double barrier model (without photo excitation) are carried out in[22] that serve as a guide for what this model could give. They show sudden rises and drops in current that even bear similarity to our experimental results that also have sharp current drops (but NOT sharp rises). These sharp drops-rises in the simulations apparently come from assuming discrete energy states which is too idealized. This mechanism is hard to reconcile with all of the experimental observations obtained so far. The NDRs are, for instance, photo-activated, which is inconsistent with a simple resonant tunnelling effect across double barriers at a surface. Furthermore, resonant tunnelling requires well-defined energy states in between tunnelling barriers, a condition for sharp transitions, but this is inconsistent with the broad TEDs obtained in Figure 5d at the transition voltage. Furthermore, the NW structures obtained by TEM appear uniform and show no evidence of double tunnelling barriers. While it is not possible to completely rule out photo-induced resonant tunnelling, a tunnelling mechanism appears unlikely in large and uniform Si NWs, such as studied here.

It is clear from the results in Figure 2 that light intensity is a key parameter for promoting the NDRs and as can be seen by the significant increase of the NDR amplitude with light intensity. Our previous work has shown that these Si NW samples have a low density of surface states and therefore they produce low dark currents, I_{dark}, especially in the saturation region[27]. As depicted in Figure 1a, the band situation is analogous to that of a diode operating in reverse bias, *i.e.* I_{dark} is mainly controlled, in the saturation regime, by carrier generation-recombination (GR) in the SCR and is given by:

$$I_{dark} = \frac{qn_iAW}{2\tau}, \qquad (1)$$

where q is the elementary charge, A is the NW cross-section area, W is the depletion width of the p-i-n junction due to field penetration, τ is the minority carrier lifetime and n_i is the intrinsic carrier concentration. I_{sat} grows linearly in the saturation region because W depends linearly on the voltage drop ($W = k\Delta V$, k is a constant), which contrasts with the known square-root dependency for bulk Si[27]. This peculiar behaviour of low dimensional materials, such as NWs, helps create large SCRs that extend deeply into the NWs. The expanding SCR counteracts in effect the increasing electric field, which prevents the field to reach at any moment the electrical breakdown, which is at 2.5×10^5V/cm for silicon[11]. Using the field drop measured by TEDs and the length of the NW, we estimate the electric field in the SCR to be roughly: $E = \Delta V_T/L = 4.5 \times 10^4\ V/cm$.

Under a continuous illumination and for short SCR, the electric field can readily separate the electron-hole pairs along the NW axis; the photo-induced electrons (holes) will preferentially diffuse towards (away from) the NW apex. This photo-generated current adds itself to the dark current, as follows:

$$I_{sat} = I_{dark} + I_{photon} \propto W\left[\beta exp\frac{-E_{gap}}{2k_BT} + \alpha\varphi\tau\right], \qquad (2)$$

where α and β are constants, φ is the photon density and τ is the carrier lifetime. This contribution explains the large sensitivity of the FE current to light intensity (Figure 2). Because of the large mobility ratio between electrons and holes ($\mu_e/\mu_h \sim 3$), we speculate that the difference in mobility further contributes to the creation of unbalanced space-charge within the SCR, which in turn affects the field distribution due to non-homogeneous carrier distributions at these interfaces. This hypothesis is schematically illustrated in Figure 6-a bottom panel.

A rough analysis of the expected field distribution suggests that the most relevant section of the SCR of the NW for building charge instabilities is near the apex. The applied field at the apex is strong as it leads to an inversion layer, the so-called $n-i$ interface (n=electron and i=intrinsic), with a small electron pocket right at the apex[27]. This electron pocket should deform locally the field lines in the high field region, as illustrated in Figure 6-a. We roughly estimate a field of about 10^7V/cm right next (outside) to the apex and 2×10^4V/cm in the NW. In effect, the internal field should be below, but close to, the dielectric breakdown of silicon (2.5×10^5V/cm)[11], which is an important factor behind device instabilities. Considering that the $p-i-n$ situation during FE can be perturbed by accumulated, yet transient, holes next to n-region at the apex, this could modulate the SCR width, giving raise to sudden current drops. That is, a change of the width of depletion region W would be associated to a transient state and the current would oscillate because of two states with different voltage drops, as illustrated in Figure 6a, lower panel.

This is a complex system which needs detailed modeling for even a basic understanding. However based on the estimates of the electric field in the SCR region, we can provide a few metrics about the dynamics of the photo-generated carriers migrating in the SCR under a field of about 4.5 V/μm. For holes and electron in a low doped Si, the associated velocities are roughly 5.5×10^6 cm/s and 9.0×10^6 cm/s, respectively[11]. The holes and electrons travel at different speeds across the depletion region, which allows for each an average distance d traveled before recombination. Using the carrier lifetime τ of 50ps estimated from the slope of the line I-ΔV at room temperature[27], we obtained distances of $d = 3\mu m$ and d=5μm for holes and electrons, respectively. Therefore, these metrics support NDRs being generated when W reaches about $3-5\mu m$. This length scale is reasonable considering that the NWs explored here are tens of μm in length and that W can easily reach scales of several micrometers in which unbalanced charge distributions are possible. The dynamics of carriers in the SCR can therefore play an important role in driving the mechanism of these photo-assisted NDRs because firstly, the photo-generated carriers existing within the SCR dominate the current, and secondly, a long SCR can support an unbalance of charges between electrons and holes and a

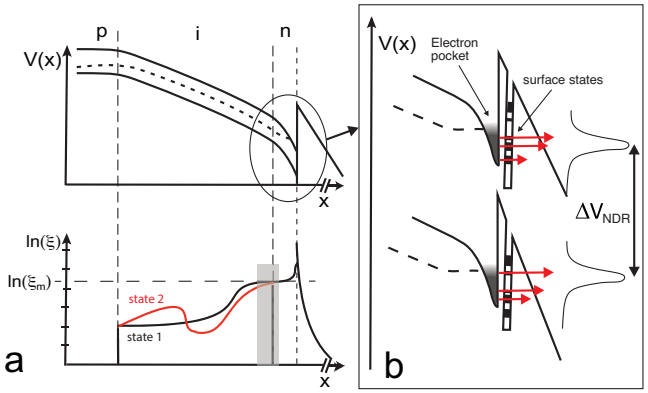

FIG. 6. Different mechanisms to explain the negative differential resistance (NDR). *a*, Scheme of the band (doping) profile of a silicon nanowire during field-emission in the saturation regime induced by the electric field ξ penetration: the doping state is n-type at the tip, intrinsic (i) in the long depletion zone, and the NW body is p-type. Bottom panel: A schematic of the field distribution along the NW and near the region at the tip according to two different states of charge distribution within the space-charge region. *b*, Scheme illustrating the influence of surface states at the surface of the emitting region on the transmitted electron distribution (TED).

space-charge transient created by the different velocities. Last but not least, the NW tip is essentially floating during FE and this sets a boundary condition that should help withstanding transient voltages induced by charged states within the NW.

IV. CONCLUSIONS

Photo-assisted field emission experiments on highly crystalline p-type silicon nanowires (NWs) have been performed to study the properties of the field-emission *IV* characteristics. The experiments reveal an original and strong double NDR in the current saturation regime, which can be modulated by temperature and laser light intensity. Mechanisms responsible of the NDR have been discussed as electronic based, while thermal mechanisms have been ruled out. These original results suggest that new functionalities and experiments in vacuum nano-electronics can be designed to explore pulsed electron sources generated by simple and stable *dc* sources. This work can potentially be expanded to design pulsed electron sources working at high repetition rates. Let us close by noting that the effect is seen on Si NWs of the most simple basic structure and there are thus a myriad of tools for its better understanding, optimisation and expansion to other geometries and materials and furthermore that Si is currently heavily explored for vacuum tip emitters[35–37].

ACKNOWLEDGMENTS

This work was carried out within the framework of the "Plateforme nanofils et nanotubes lyonnaise". R.M. acknowledges support from Canada Research Chair and NSERC under grants RGPIN-2019-06545 and RGPAS-2019-00050 and Canada Research Chair.

DATA AVAILABILITY STATEMENT

The data that support the findings of this study are available in the Supporting Information file and from the corresponding author upon reasonable request.

SUPPLEMENTARY MATERIAL

See supplementary material at [URL will be inserted by AIP Publishing] for 1) Extra Figures, 2) a schema of the UHV system and 3) Calculation of Laser Heating at $1 W/cm^2$.

AUTHOR DECLARATIONS

The authors declare no competing financial interest.

M.C., A.D., P.V., A.A. and R.M. performed the experiments; M.C., R.M. and S.T.P. wrote the paper, designed the experiments and analyzed the results; C.S.C. produced the Si NWs used in this study; M.C., R.M., P.V. and P.P. prepared the samples; S.P. carried out calculations of thermal self-heating and mechanical resonance frequencies; R.M and S.T.P. supervised the work. All authors contributed to the scientific discussions, manuscript preparation, and final version.

[1] A. H. Zewail, Science **328**, 187 (2010).
[2] A. Feist, K. E. Echternkamp, J. Schauss, S. V. Yalunin, S. Schafer, and C. Ropers, Nature **521**, 200 (2015).
[3] M. Kruger, M. Schenk, and P. Hommelhoff, Nature **475**, 78 (2011).
[4] M. F. Ciappina and *et al.*, Rep. Prog. Phys. **80**, 054401 (2017).
[5] B. J. Siwick, J. R. Dwyer, R. Jordan, and R. J. D. Miller, Science **302**, 1382 (2003).
[6] T. Ishikawa and *et al.*, Science **350**, 1501 (2015).
[7] M. Gulde, S. Schweda, G. Storeck, M. Maiti, H. K. Yu, A. M. Wodtke, S. Schfer, and C. Ropers, Science **345**, 200 (2014).
[8] L. Hudanski, E. Minoux, L. Gangloff, K. B. K. Teo, J.-P. Schnell, S. Xavier, J. Robertson, W. I. Milne, D. Pribat, and P. Legagneux, Nanotechnology **19**, 105201 (2008).
[9] L. Sabaut, P. Ponard, J.-P. Mazellier, and P. Legagneux, J. Vac. Sci. Tech. B **34**, 02G101 (2016).
[10] A. Ayari, P. Vincent, S. Perisanu, M. Choueib, M. Gouttenoire, M. Bechelany, D. Cornu, and S. T. Purcell, Nano Letters **7**, 2252 (2007).
[11] S. M. Sze, *Physics of Semiconductor Devices* (Wiley Interscience, New Jersey, 1969) pp. 96–104.
[12] J. B. Gunn, IEEE J. Quantum Electron. **1**, 88 (1963).
[13] C. L. Ho, M. C. Wu, W. J. Ho, and J. W. Liaw, Appl. Phys. Lett. **74**, 4008 (1999).
[14] F. Capasso, K. Mohammed, and A. Y. Cho, IEEE J. Quantum Electron. **QE-22**, 1853 (1986).
[15] F. Chen, B. Li, and K. D. Feng, Appl. Phys. Lett. **80**, 3271 (2002).
[16] M. P. Shaw, V. V. Mitin, E. Scholl, and H. L. Grubin, *The physics of instabilities in solid state electron devices* (Plenium Press, New York, 1992) pp. 1–11.
[17] H. W. Tsang, S. J. Menley, V. Stolojan, and S. R. P. Silva, Appl.Phys.Lett. **89**, 193103 (2006).
[18] S. Johnson, U. Zulicke, and A. Markwitz, J. Appl. Phys. **101**, 123712 (2007).
[19] O. Yilmazoglu and *et al.*, J. Vac. Sci. and Technol. B **30(4)**, 042203 (2007).
[20] W. Zhao and *et al.*, Appl. Phys. Lett. **30(4)**, 152110 (2007).

[21] R. R. Y. R. A. H. V. S. M. Semenenko, S. Antonin and A. Evtukh, .
[22] V. Litovchenko, A. Evtukh, Y. Kryuchenko, N. Goncharuk, O. Yilmazoglu, K. Mutamba, H. L. Hartnagel, and D. Pavlidis, J. Appl. Phys. **96**, 867 (2004).
[23] Y. Ishida, A Inoue and H. Fujiyasu, Appl.Phys.Lett. **86**, 183102 (2005).
[24] R. H. Wang, W. Zhao, , and H. Yan, Sci. Rep. **7**, 43625 (2017).
[25] E. Lefeuvre, K. H. Kim, M. Chatelet, D. Pribat, and C. S. Cojocaru, Thin Solid Films **519**, 4603 (2011).
[26] S. T. Purcell, P. Vincent, C. Journet, and V. Binh, Phys.Rev.Lett. **89**, 276103 (2002).
[27] M. Choueib, R. Martel, C. S. Cojocaru, A. Ayari, P. Vincent, and S. T. Purcell, ACS Nano. **6**, 7463 (2012).
[28] N. P. Blanchard, A. Nigues, M. Choueib, S. Perisanu, A. Ayari, A. Poncharal, S. T. Purcell, A. Siria, and P. Vincent, Appl. Phys. Lett. **106**, 193102 (2015).
[29] R. J. Arthur, J. Appl. Phys. **36**, 3221 (1965).
[30] L. M. Baskin, O. I. Lvov, and G. N. Fursey, Phys. Status Solidi B **47**, 49 (1971).
[31] M. Choueib, A. Ayari, P. Vincent, M. Bechelany, D. Cornu, and S. T. Purcell, Physical Review B **79**, 075421 (2009).
[32] M. Choueib, A. Ayari, P. Poncharal, C. Journet, C. S. Cojocaru, R. Martel, and S. T. Purcell, Appl. Phys. Lett. **99**, 072115 (2011).
[33] H. W. Tsang, S. J. Menley, V. Stolojan, and S. R. P. Silva, Appl. Phys. Lett. **89**, 193103 (2006).
[34] Y. Ishida, A Inoue and H. Fujiyasu, Appl.Phys.Lett. **86**, 183102 (2005).
[35] C. Langer, V. Bomke, M. Hausladen, R. Lawrowski, C. Prommesberger, M. Bachmann, and R. Schreiner, J. Vac. Sci. Technol. B **38**, 013202 (2020).
[36] S. Guerrera and A. Akinwande, Nanotechnology **27**, 295302 (2016).
[37] H. Shimawaki, M. Nagao, Y. Neo, H. Mimura, F. Wakaya, and T. M, Appl. Phys. Lett. **109**, 183106 (2016).

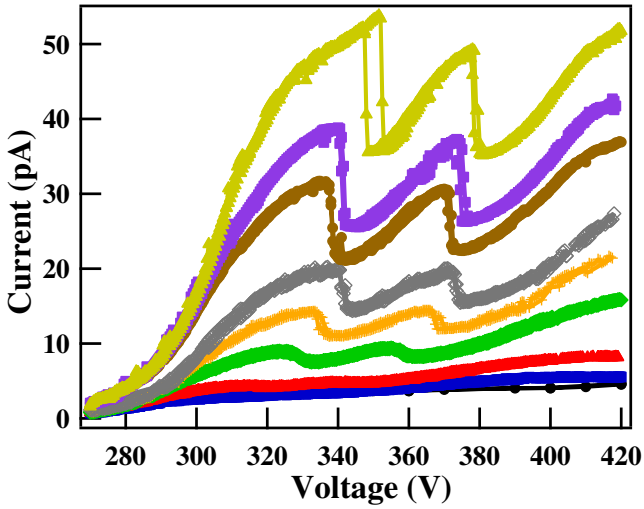

FIG. 7. Abstract Figure